International Journal of Plasticity 123 (2019) 196–207

Contents lists available at ScienceDirect

International Journal of Plasticity

journal homepage: www.elsevier.com/locate/ijplas

Extra strengthening in a coarse/ultrafine grained laminate: Role of gradient interfaces

Y.F. Wang[a,b], M.S. Wang[a], X.T. Fang[b], F.J. Guo[a], H.Q. Liu[a], R.O. Scattergood[b], C.X. Huang[a,*], Y.T. Zhu[b,c]

[a] School of Aeronautics and Astronautics, Sichuan University, Chengdu, 610065, China
[b] Department of Materials Science and Engineering, North Carolina State University, Raleigh, NC, 27695, USA
[c] Nano and Heterogeneous Structural Materials Center, School of Materials Science and Engineering, Nanjing University of Science and Technology, Nanjing, 210094, China

ARTICLE INFO

Keywords:
Heterogeneous structure
Gradient interface
Strain gradient
Geometrically necessary dislocation (GND)
Synergetic strengthening

ABSTRACT

The interfaces introduced in metals by heterostructural design play crucial roles in mechanical behaviors. Here the effect of gradient interfaces on mechanical behavior was investigated in a laminated Cu–30Zn sample composed of coarse-grained and ultrafine-grained layers. Tensile tests revealed a superior strength-ductility synergy with extraordinary strengthening and work hardening. By combining the measurements of height contour and strain distribution using digital image correlation, the development of strain gradient was detected in the near-interface zone during tension, which was caused by the mechanical incompatibilities across interfaces and the synergetic constraint between layers. The intensity of strain gradient in the near-interface zone increased with tensile strain, which was accommodated by the accumulation of geometrically necessary dislocations, thereby resulting in extra back stress and dislocation strengthening.

1. Introduction

Heterostructured metal is a new class of materials with unique structural and mechanical properties (Wu and Zhu, 2017). Their microstructures are characterized with multiple domains with dramatically different strength. The inter-domain interfaces can be gradient or sharp (Huang et al., 2018; Park et al., 2018; Wu et al., 2015, 2014a). Due to the synergetic interaction among mechanically incompatible domains, their mechanical properties are usually superior to what is predicted by the rule of mixture (Cheng et al., 2018; Wang et al., 2018c; Wu et al., 2015, 2014b). In recent years, tailored strength-ductility synergy and enhanced work hardening have been achieved in several types of heterostructures, including the laminate (Huang et al., 2018; Ma et al., 2016; Wu et al., 2017), gradient (Cheng et al., 2018; Fang et al., 2011; Wang et al., 2018b; Wei et al., 2014; Wu et al., 2014a), hierarchical lamellar (Li et al., 2018; Wu et al., 2015), harmonic (Ming et al., 2019; Park et al., 2018) and partially recrystallized (Wu et al., 2019) structures.

Critical questions arise on where in such heterogeneous structures is the improved strength and strain hardening originated and how the heterogeneous domains deform synergistically. Although there are big differences in the detailed microstructures of these heterogeneous materials, the fundamental deformation principles, such as inhomogeneous deformation across domain interfaces and hierarchical strain/stress partitioning among domains, might be universal (Wu and Zhu, 2017). The partitioning and inhomogeneous

* Corresponding author.
E-mail address: chxhuang@scu.edu.cn (C.X. Huang).

https://doi.org/10.1016/j.ijplas.2019.07.019
Received 5 March 2019; Received in revised form 6 July 2019; Accepted 28 July 2019
Available online 30 July 2019
0749-6419/

accumulation of strain are associated with the formation of strain gradient across domain interfaces in order to maintain strain continuity (Ashby, 1970; Huang et al., 2018). As proposed and simulated in gradient structure, plastic strain gradient could be accumulated with the migration of elastic/plastic interface during straining (Wu et al., 2014a; Zeng et al., 2016). Pronounced gradient strain distribution was simulated in the laminate composed of multiple layers with grain-size gradient in each layer (Lyu et al., 2017).

It is also recognized that the plastic strain gradient around interfaces needs to be accommodated by the accumulation of geometrically necessary dislocations (GNDs), which is effective in developing internal stresses (Ashby, 1970; Kassner et al., 2013; Mughrabi, 2006). This unusual dislocation activity provides an opportunity to promote extraordinary strengthening and strain hardening, and change the stress-strain behavior of componential domains (Cheng et al., 2018; Park et al., 2018; Yang et al., 2016). For example, the improved strain hardening and strengthening of gradient and laminate heterostructures can be theoretically predicted by incorporating the effects of GNDs and long-range back stress around interfaces (Li et al., 2017b, 2017a). Therefore, the interfaces between domains are believed to significantly affect the strain accommodation and mechanical responses of heterostructures. On the other hand, the heterostructured interfaces themselves may have direct effects on the nucleation and pile-up of dislocations as well (Mayeur et al., 2015; Murr, 2016; Wang et al., 2014).

Early works on the sharp interfaces in the nanostructured (NS)/coarse-grained (CG) laminates have revealed a strain gradient-dominated interface-affected-zone where extra GNDs were accumulated (Huang et al., 2018; Ma et al., 2016). However, for some other heterostructures, such as gradient materials and the engineering composites synthesized by welding, the interface between heterogeneous domains generally has transitional microstructure, i.e., a gradient interface (Wu et al., 2014a; Zhu et al., 2017). Such gradient interface avoids the early formation of serious stress concentration and local cracking problems that are typical in a sharp interface, and is expected to produce wider affected zone and be more efficient in enhancing mechanical performances. In spite of the above progresses, direct visualization and quantitative analysis for the plastic behaviors of gradient interface are still lacking. These are also essential for understanding the fundamental deformation and strengthening mechanism of heterogeneous materials.

In this paper we report a CG/ultrafine-grained (UFG) laminate structure with two discrete gradient interfaces. The configuration and evolution of 3D strain gradient near gradient interface were quantitatively visualized using height contour measurement and in-situ digital image correlation (DIC). The formation of strain gradient and its effect on strengthening and strain hardening behaviors will be discussed.

2. Experimental methods

Friction stir processing (FSP) was used to fabricate the laminate samples with gradient interfaces. An annealed Cu-30 wt%Zn plate with a thickness of 5.6 mm was selected as CG base metal (BM). The advantage of this material is its low stacking fault energy and proper melting temperature, which are conducive to the formation of recrystallized UFG in the string zone (SZ) during FSP (Chang et al., 2004; Wang et al., 2018a). The FSP tool has a shoulder diameter of 12 mm and an unthreaded cylindrical pin in length of 1.8 mm and diameter of 3 mm. Two FSP procedures were symmetrically conducted on both sides of the plate under flowing water at a constant rotational speed of 1400 rpm and a traverse speed of 200 mm/min. The as-processed plate was annealed at 250 °C for 48 h in order to relieve residual stress. Fig. 1(a) shows the cross-sectional morphology of the as-prepared sample observed by scanning

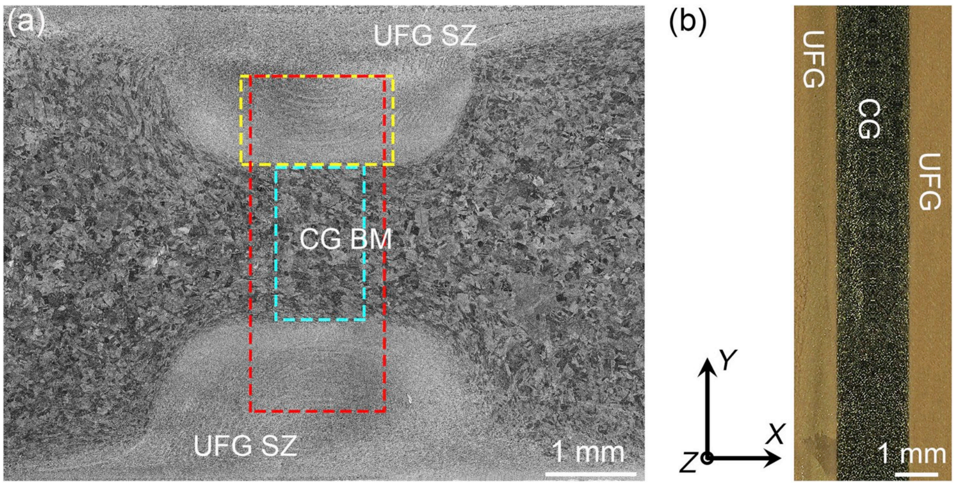

Fig. 1. (a) Scanning electron morphology of the cross-section of FSP processed heterogeneous structure, showing a CG layer sandwiched between two UFG zones. Colored frames illustrate the cross-section of heterogeneous laminate (red), freestanding CG (light blue) and UFG (yellow) samples used for tensile testing, respectively. (b) An optical overview on the lateral surface (18 × 3.7 mm^2 surface) of the heterogeneous laminate sample, showing straight interfaces between layers. In the coordinate, Y is the tensile loading direction; X and Z are the thickness and the width directions of laminate sample, respectively. (For interpretation of the references to color in this figure legend, the reader is referred to the Web version of this article.)

electron microscope (SEM). There is clear metallurgic contrast between BM and SZ domains, suggesting great difference in their microstructures. As verified later, homogeneous UFG was formed in the SZ.

The heterogeneous microstructures were characterized using transmission electron microscopy (TEM) and electron back-scattered diffraction (EBSD). EBSD samples were mechanically polished using standard metallographic techniques and then electronically polished to remove the strained surface layer. TEM foils were accurately extracted from exact positions using the focused ion beam (FIB) lift-out technique. TEM observation was performed in a FEI Tecnai G2 T20 microscope at 200 KV.

Dog-bone shaped tensile specimens with a gauge length of 18 mm were machined parallel to the processing direction in as-FSP processed plate. The colored frames in Fig. 1(a) show the position and dimension of the gauge cross-section of tensile samples. The cross-sectional dimension of heterogeneous laminate (red), freestanding CG (light blue) and UFG (yellow) samples are $1.5 \times 3.7\,mm^2$, $1 \times 1.7\,mm^2$ and $1.7 \times 1\,mm^2$, respectively. Fig. 1(b) shows the optical morphology of the lateral surface of laminate sample. Clearly, it is composed of a CG core layer and two UFG surface layers with a thickness ratio of 1:1.7:1. The thickness and width of all samples were precisely controlled by polishing off redundant surface. Tests for each type of sample were performed three times at a nominal strain rate of $5 \times 10^{-4}\,s^{-1}$.

In order to evaluate the mechanical incompatibility and the deformation-induced hardening in the near-interface zone, microhardness measurements were carried out across the interface between SZ and BM on both samples before and after tensile deformation, using a load of 25 g. All samples for microhardness testing were first mechanically polished to achieve a mirror-like surface, and then electrochemically polished at a relatively low voltage to remove the strained top-most surface layer and expose the layer boundary. To confirm reproducibility, the hardness distribution for each type of sample was repeatedly measured at four independent positions.

The height contours on the lateral surface (Fig. 1(b)) of the laminate samples before and after tensile test were measured using a Bruker Contour-I white light interferometry in a vertical scanning mode. The height resolution in depth is about 20 nm. In-situ 2D DIC was also conducted on the lateral surface of laminate sample, using a short-focus optical lens. Before performing DIC imaging, a random pattern was prepared by spraying black paints on white background.

3. Results

3.1. Microstructural heterogeneity and gradient interface

As the cross-sectional morphology shown in Fig. 1(a), there is a well-defined straight outline on the bottom of the SZ. Fig. 2(a) is a representative TEM image of SZ, showing equiaxed UFG structure with clear and sharp grain boundaries. FSP is a severe thermal-plastic deformation process, during which subdivision and fragmentation of parent large grains and dynamic recrystallization to form new small grains occurred simultaneously (Wang et al., 2018a). In this study, the formation of UFG microstructure can be primarily attributed to the low stacking fault energy of material and the fast cooling rate under flowing water during processing (Chang et al., 2004).

Fig. 2(b) shows the microstructural details between SZ and BM. A continuous transition in grain size from recrystallized UFG to

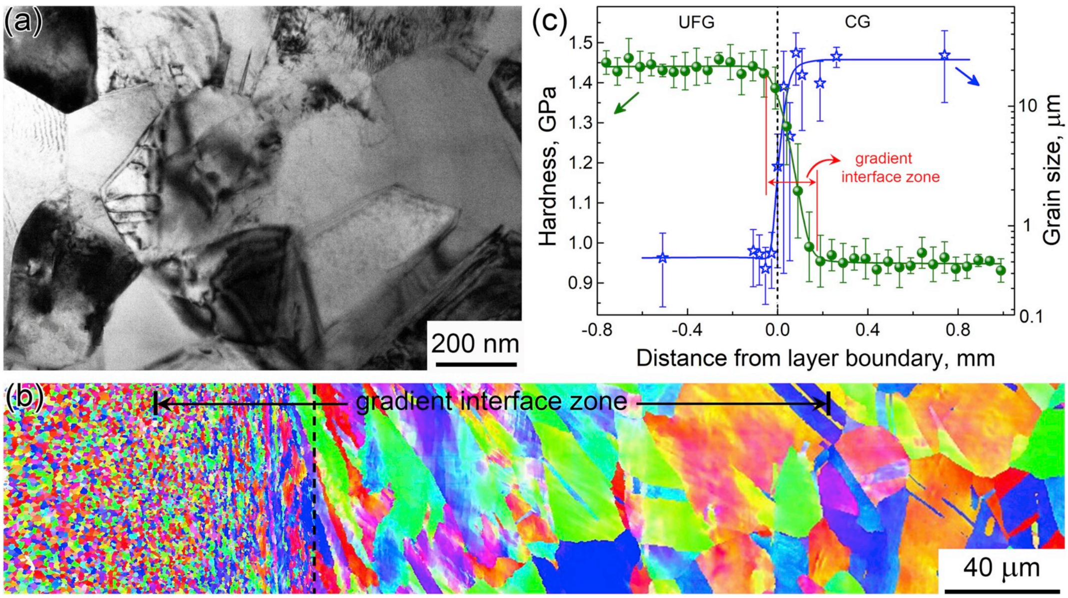

Fig. 2. The microstructural and mechanical heterogeneities of FSP processed sample. (a) Typical TEM image in the SZ. (b) An EBSD morphology showing the gradient interface between CG and UFG layers. (c) Variation of the average hardness and grain size measured across gradient interface zone. Every hardness datum was averaged from 4 indentations. The black dotted lines in (b) and (c) denote the layer boundary.

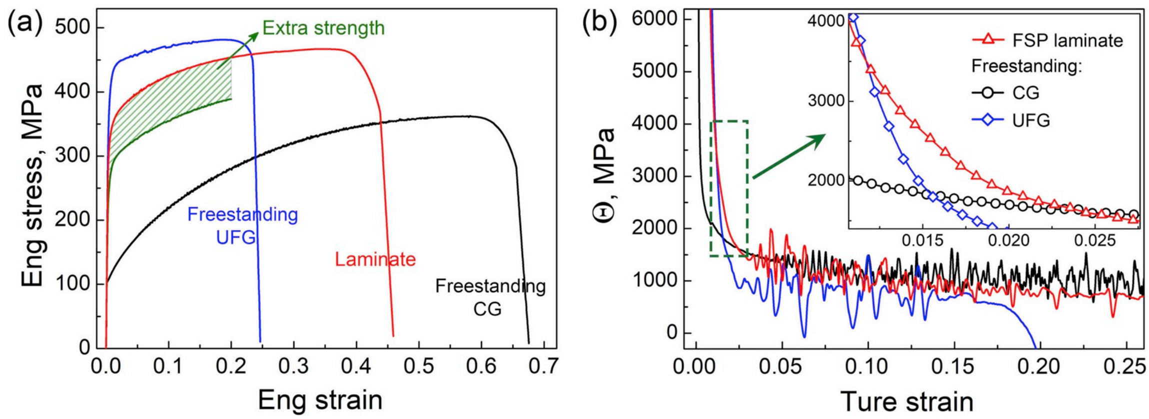

Fig. 3. Uniaxial tensile behaviors of CG/UFG laminate, freestanding CG and UFG samples: (a) engineering stress-strain curves; (b) strain hardening rate (Θ) vs. true strain. The green curve in (a) is the predicted response for CG/UFG laminate sample basing on rule of mixture. The inset in (b) is the magnified curve at low strains where the CG/UFG laminate sample exhibits extremely high Θ. (For interpretation of the references to color in this figure legend, the reader is referred to the Web version of this article.)

plastically elongated CG and then equiaxed CG is produced, forming a gradient transition zone between SZ and BM. The variation of average hardness and grain size were statistically measured across the boundary between UFG SZ and CG BM. As shown in Fig. 2(c), the hardness within both UFG and CG layers is rather homogeneous, while transitions with a discrepancy of ~0.48 GPa appears between them. The average grain size of the UFG and CG layers determined from EBSD images are ~25 μm and ~0.54 μm, respectively. The black dotted line in Fig. 2(c) marks the starting point of the precipitous drop of hardness, which corresponds strictly to the position in microstructure indicated by black dotted line in Fig. 2(b) where the grain size increases sharply. This geometric position can be easily located by metallographic observation, which is referred to as the boundary of UFG and CG layers. Note that the widths of freestanding UFG and CG tensile samples were precisely polished by referring to this layer boundary. The region with hardness and microstructure transition is defined as the gradient interface zone between CG and UFG layer.

Such heterogeneous laminate structure with discrete gradient interfaces avoids the tracking problem of transferable interface in gradient structure (Zeng et al., 2016). Therefore, the CG/UFG laminate specimen cut as the red cross-section in Fig. 1 can be viewed as a model sample for studying the plastic behavior around a single gradient interface.

3.2. Synergetic strengthening and strain hardening

Fig. 3(a) shows the tensile stress-strain curves for CG/UFG laminate, freestanding CG and UFG samples. The ultimate strength of CG/UFG laminate is measured as 467 MPa, which is comparable to that of pure UFG sample (481 MPa). Such a surprising strength is superior to what is predicted using the volume fraction-based rule of mixture (green curve in Fig. 3(a)) (Wu et al., 2014b). Accordingly, a shadow region could be drawn between the prediction and experimentally measured curves, as seen in Fig. 3(a). This indicates an extra flow stress achieved in CG/UFG laminate sample, demonstrating a considerable synergetic strengthening in such heterogeneous structure (Wang et al., 2018b; Wu et al., 2014b). The extra yield strength at is measured as 63 MPa, which accounts for 19.8% of the flow strength.

The comparison of strain hardening behaviors is shown in Fig. 3(b). Surprisingly, the strain hardening rate (Θ) of laminate sample is higher than that of both freestanding UFG and CG samples at a low plastic strain stage (~1%–2.5%). Interestingly, the strain regime for the high strain hardening rate is consistent with that (1.8%–3.2%) of Θ-up-turn in gradient IF steel (Wu et al., 2014a). This implies that some underlying mechanisms such as complex stress/strain states induced by mutual constraint between layers should be the same in these two structures.

Since the strain hardening of laminate sample is very graceful, one may wonder whether the uniform elongation is also larger than the prediction calculated from rule of mixture (Ma et al., 2015). However, the experimental result (29.6% ± 1.7%) is approximately equal to the prediction (30.3%). This can be attributed to the high stress concentration at interface. It was revealed in CG/UFG heterostructured Cu samples (Wang et al., 2019) that the uniform elongation and fracture of laminates with gradient interface are dominated by the damages developing from interface, rather than that in the harder layer. During straining, the triaxial stress concentration induced by synergetic interaction between layers is capable of promoting plastic damages (such as micro voids) preferentially from interface, which leads to premature termination of uniform elongation before the necking of harder layer.

3.3. Height profile and strain gradient across interface

It is interesting to find that the heterostructured layers in CG/UFG laminate (Fig. 1(b)) after tension exhibits remarkable difference in lateral height contour. Fig. 4(a) and (b) show the 3D height profiles measured on the lateral surface before and after tensile deformation, respectively. Obviously, the initial electrochemically polished surface has no height difference between layers except

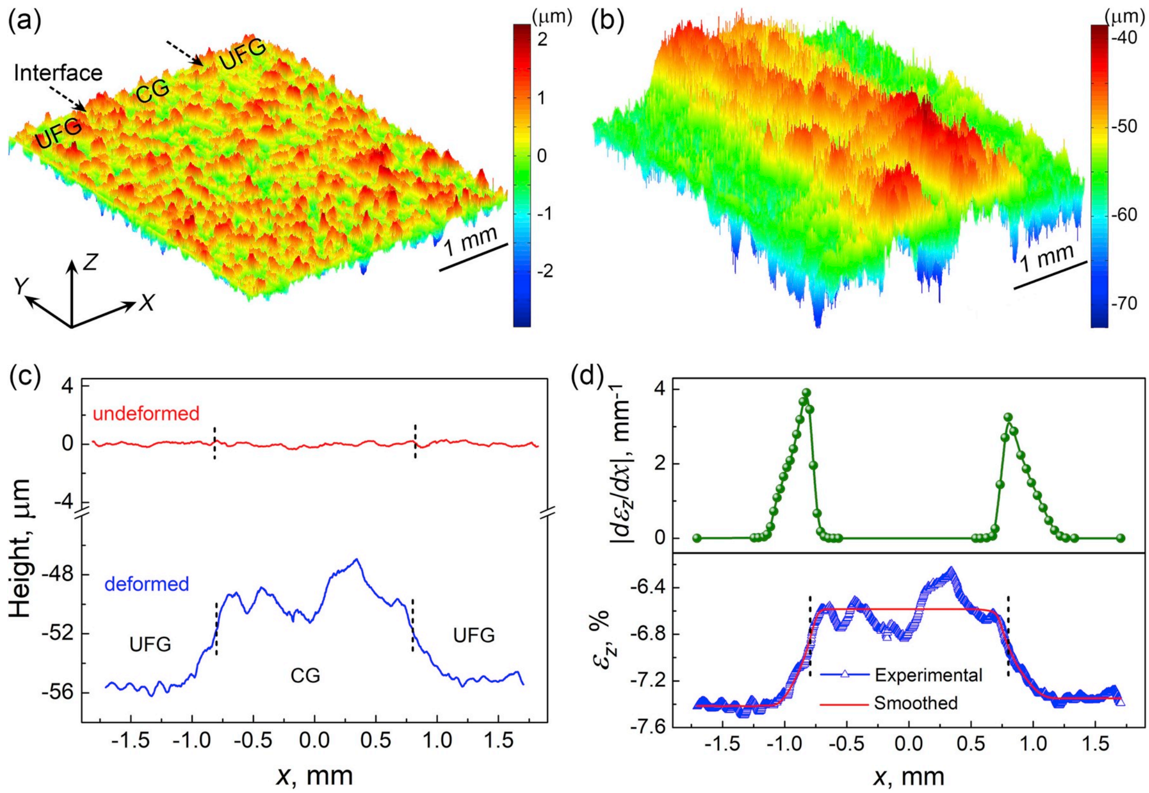

Fig. 4. 3D height contour measured on the lateral surface of CG/UFG laminate sample: (a) before tension, (b) after tensile testing to a strain of 14%. (c) The distribution of statistical average height as a function of sample thickness (*X*). (d) The distribution of strain ε_z and strain gradient $|d\varepsilon_z/dx|$ deduced from the height profile in (c). The dotted arrows and lines mark the position of layer boundary.

minor surface roughness. However, the central CG layer in the deformed sample is much higher than the UFG layers on both sides, as seen in Fig. 4(b). These height contours were statistically averaged along the tensile direction (*Y*) and plotted versus the sample thickness (*X*) in Fig. 4(c). The black dotted lines in Fig. 4(c) denote the position of layer boundaries, which were accurately located by polishing off the surface roughness firstly and then metallographic examining using SEM. It is seen that the height difference across layer boundary is as high as ~6 μm.

The shrinking strain in sample width direction ε_z, i.e. the lateral strain parallel to the interface, can be deduced from the height profiles (Wu et al., 2014a). As the blue curve plotted in Fig. 4(d), the surface UFG layers have higher $|\varepsilon_z|$ than the central CG layer, and ε_z changes gradually in near-interface zone. The green curve in Fig. 4(d) represents the distribution of strain gradient $|d\varepsilon_z/dx|$ across interfaces, which was deduced from the smoothed ε_z (red curve). It is obvious that the near-interface zones present pronounced strain gradient, and the average width of strain gradient zones (~500 μm) is much larger than that (~250 μm) of the gradient interface (Fig. 2(b) and (c)). It is technically difficult to locate the exact position of strain gradient peak because the derivative of smoothed strain distribution is varied with the assumed mathematical function of smoothing. But it is certain that the peak is at or adjacent to the layer boundary, where a remarkable change in hardness and grain size occurs (Fig. 2). Moreover, the zone with strain gradient in the UFG side is wider than that in the CG side, suggesting a higher efficiency in accommodating strain gradient for the latter.

3.4. DIC and strain gradient across interface

2D DIC experiments were conducted on the lateral surface to extract the in-plane strains, i.e. the normal strains in the tensile direction ε_y and the sample thickness direction ε_x. The digital speckle image covers the effective correlation area of 1630 × 382 pixel^2 with a spatial resolution of 9.7 μm/pixel (Fig. 5(a)). Fig. 5(b) shows the detailed distribution of gray scale with clear contrast in a single correlation window. This high-quality speckle pattern is an essential prerequisite for accurate strain calculation.

Fig. 6(a) and (b) are the typical contours of ε_y and corresponding ε_x mapped at various tensile strains. Fig. 6(c) and (d) show the evolution of ε_y and ε_x with increasing tensile strain, respectively, which were statistically averaged along the tensile direction and plotted as a function of thickness. Several general features can be observed from these strain distributions. First, ε_y distributes homogeneously along both the tensile direction *Y* and the thickness direction *X*, confirming that the UFG layers elongated concurrently with CG core in the laminate structure (Wu et al., 2017). Second, the CG layer exhibits higher ε_x than the UFG layers, as seen in Fig. 6(d). Third, ε_x exhibits obvious gradient distribution across the interfaces, i.e. high $|d\varepsilon_x/dx|$ in near interface zones

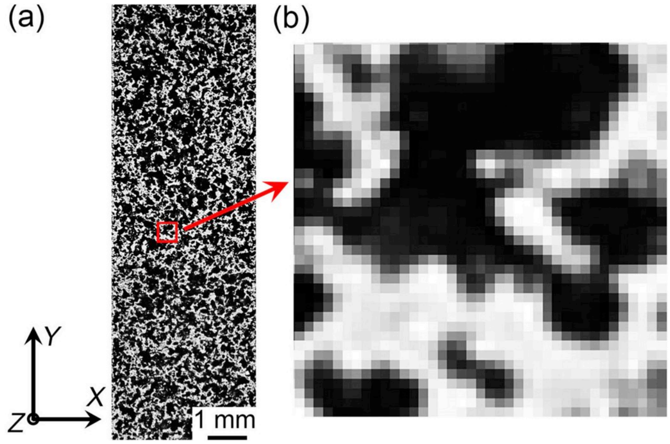

Fig. 5. DIC speckle image taken from the lateral surface of CG/UFG laminate sample: (a) typical speckle pattern; (b) detailed distribution of gray scale in a single correlation window (40 × 40 pixel^2).

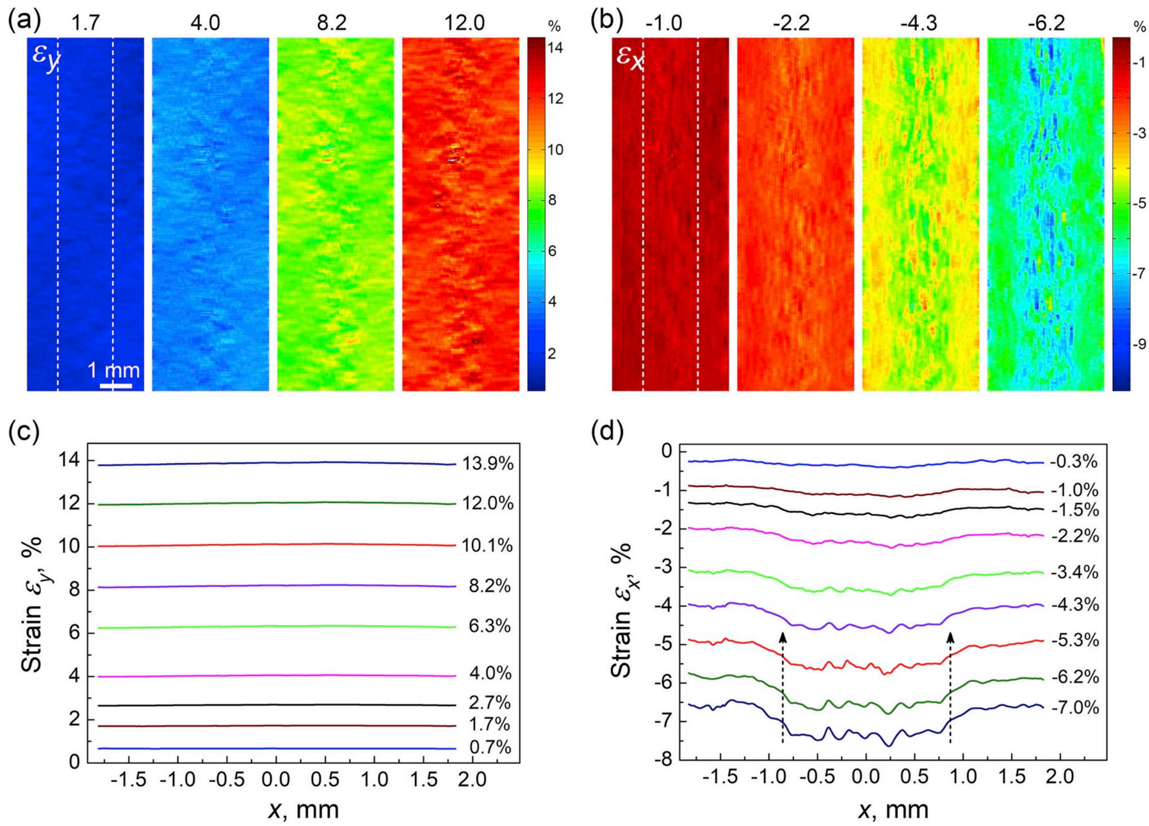

Fig. 6. (a) and (b) are the contours of strain ε_y and ε_x mapped at different tensile strains, respectively. (c) and (d) are the distribution of statistical average strain ε_y and ε_x plotted as a function of distance from the center of thickness, respectively. The dotted arrows and lines mark the position of layer boundaries.

(Fig. 6(b) and (d)). Furthermore, the position and width of the gradient zone of strain ε_x are consistent well with that of ε_z revealed in Fig. 4(d).

Fig. 7(a) shows the plot of strain gradient ($|d\varepsilon_x/dx|$) against the sample thickness, which is extracted from the distribution of ε_x. The evolution of the width (W) and intensity (I) for two strain gradient peaks are plotted in Fig. 7(b). As shown, the intensity I increases with increasing applied strain. Since the strain gradient is resulted from the mutual constraint between incompatible domains, the persistent increase of I suggests that the interaction between CG and UFG layers was never interrupted or attenuated during uniform elongation. Surprisingly, the width W (~500 μm) remains largely constant during straining. One possible reason for

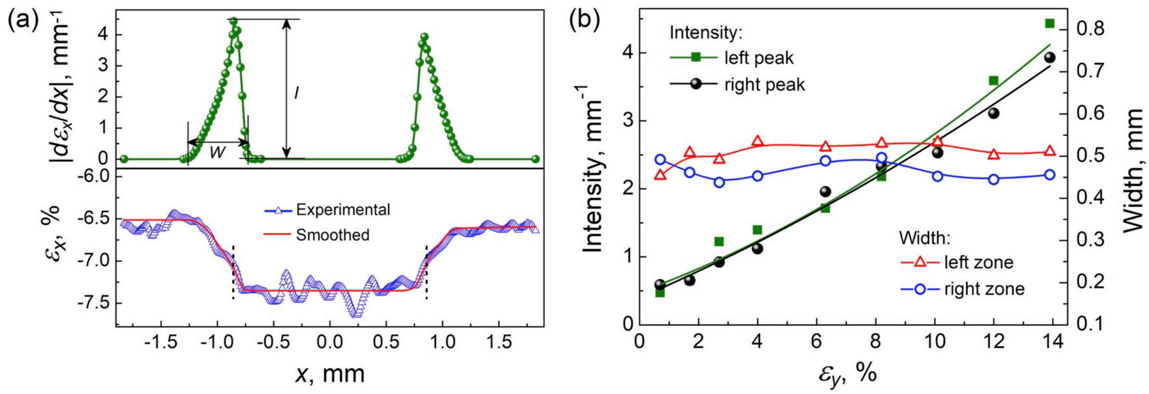

Fig. 7. (a) The distribution of strain ε_x and strain gradient $|d\varepsilon_x/dx|$ at a tensile strain of 13.9%. (b) The evolution of the intensity (I) and width (W) of strain gradient peaks.

this puzzle is that the zone for the accumulation of GNDs induced by the mutual interaction across the gradient interface is limited within ~500 μm. This is similar to the situation in CG/NS laminates that the strain gradient zone around sharp interfaces maintained a constant width during tension (Huang et al., 2018; Ma et al., 2016).

4. Discussion

The inhomogeneous distribution of strains across the gradient interface measured by height contour measurement and DIC strain characterization confirm the validity of each other, according to the criterion that metals keep a constant volume during plastic deformation, i.e. $\varepsilon_y = -(\varepsilon_x + \varepsilon_z)$. Note that the strain gradient of two lateral shrinking strains only exists in the X direction with structural heterogeneity. This demonstrates that such strain gradients are inherent to the heterogeneous structures.

4.1. Formation of strain gradient across gradient interface

The mechanical incompatibilities induced by structure heterogeneity, such as the discrepancies in elastic limit, strain hardening capability and propagation of plastic damage, lead to synergistic constraint between CG and UFG layers during deformation (Wang et al., 2018c; Wu et al., 2017, 2014a). This is capable of reshaping the strain path of component layers by hierarchical strain partitioning between them (Huang et al., 2016). In order to maintain the strain continuity and avoid the formation of stress singularity in the near-interface zone, the formation of strain gradient is inevitable (Ashby, 1970; Lu et al., 2019; Mughrabi, 2006).

In the yielding stage, the big difference in elastic limit across interface led to a long elastic-plastic transition process, during which the fast shrinking of yielded CG in near-interface zone can be suppressed by a lateral tensile constraint from elastic UFG layer, i.e. elastic/plastic interaction (Wang et al., 2018c; Yang et al., 2019; Zeng et al., 2016). At the end of yielding, the discrepancy of lateral elastic strain between CG and UFG layer is calculated to be about 0.05%.

After yielding, the CG and UFG layers deformed plastically together. However, the mechanical incompatibilities are still prevalent across the interfaces. Here, several reasons associated with structure heterogeneity are summarized for the prevalence of strain discrepancy and the accumulation of strain gradient during the uniform plastic deformation stage. Firstly, the UFG layers have an earlier strain localization tendency due to their relatively low strain hardening capability. Such unstable tendency is incompatible with the stable plastic deformation of CG core, and can be constrained by the latter (Wu et al., 2014a). This interaction process contributes to the accumulation of strain gradient near the CG/UFG interfaces.

Secondly, the propagation of early damage in UFG layers, such as micro strain concentration bands, can be effectively passivated and/or impeded by the gradient interface (Chen et al., 2008; Huang et al., 2016). This procedure can make the propagation of damage preferentially along the direction parallel to interfaces, i.e., reshaping the strain path of UFG layer by promoting the shrinking strain along direction Z (Fig. 4). It is for this reason that the ε_z in UFG layers is higher than that in CG layer (Fig. 4(d)). As a result, the strain discrepancy across interface is enhanced, and the intensity of strain gradient is further increased.

4.2. GNDs pile-up across gradient interface

Following the plastic model of compatible non-homogeneous deformation proposed by Ashby (1970), the density and arrangement of GNDs in strain gradient zone can be derived by inserting an array of dislocations to compensate the excess strain and/or displacement (Cheng et al., 2018; Li et al., 2017b, 2017a). For the zone with a known inhomogeneous distribution of plastic strain, the density of GNDs, ρ_G, can be calculated by (Gao et al., 1999)

$$\rho_G = \eta / b \tag{1}$$

where b is the Burgers vector. η is the equivalent strain gradient which is expressed as

$$\eta = \frac{1}{2}\sqrt{\eta_{ijk}\eta_{ijk}} \tag{2}$$

and

$$\eta_{ijk} = u_{k,ij} \tag{3}$$

where η_{ijk} and u_k are the strain gradient and the displacement tensors, respectively. In the current study, the statistically averaged ε_y is uniformly distributed in the three axial directions, and ε_x and ε_z exhibit gradient in the *X* direction only (Figs. 4 and 6), i.e. $\varepsilon_y = C$, $\varepsilon_x = h(x)$ and $\varepsilon_z = -C-h(x)$. Therefore, the first-order approximation of displacement functions *u* in *X*, *Y* and *Z* directions can be written as

$$u_x = \int h(x)\, d_x \tag{4.1}$$

$$u_y = \mathrm{C}y \tag{4.2}$$

and

$$u_z = -\mathrm{C}z - h(x)z \tag{4.3}$$

where C is a constant. The non-zero components of strain gradient η_{ijk} derived from Eqs. (3) and (4) are

$$\eta_{xxx} = -\eta_{xzz} = -\eta_{zxz} = h'(x) \tag{5.1}$$

and

$$\eta_{xxz} = -h''(x)z \tag{5.2}$$

Note that the hydrostatic part of above η_{ijk} components is also equal to 0, which is another necessary condition for plastic incompressibility. Submitting Eqs. (5) and (2) into Eq. (1) leads to the detailed function of ρ_G as follow

$$\rho_G = \sqrt{3h'^2(x) + h''^2(x)z^2}/2b \tag{6}$$

By slicing the strain gradient zone into *n* unit layers, one can assume that for each unite layer GNDs are uniformly arranged in the plane paralleled with the interface (Li et al., 2017a, 2017b). This assumption is a valid approximation since there is no in-layer structure inhomogeneity. Therefore, the $h''^2(x)z^2$ in Eq. (6) can be interpreted as a second-order small component that is ignorable. The $h'(x)$ in Eq. (6) was calculated numerically by differencing the smoothed data matrix of ε_x (Figs. 6(d) and 7(a)) along *X* direction. The calculated ρ_G is plotted as the distance from thickness center in Fig. 8, which shows pronounced increase of GND pile-ups in near-interface zones. This is similar to the GND pile-ups around the sharp interface between CG and NS layers (Huang et al., 2018; Ma et al., 2016). These results confirm the roles of gradient interface in undertaking strain gradient and accumulating GNDs, i.e., accommodating strain inhomogeneity. It should be noted that the above discussion is based on the assumption that all of the strain gradient is accommodated by the GNDs, a concept that has been well accepted (Ashby, 1970; Gao et al., 1999).

4.3. Dislocation density gradient in the near-interface zone of UFG layer

To experimentally verify the inhomogeneous distribution of dislocation density in the near-interface zone, the variation of microstructures in UFG layer with increasing distance from layer boundary were comparatively investigated in the laminates before and after tensile deformation.

Fig. 9(a–c) show the typical TEM micrograph of the as-received UFG regions with a distance of ~20 μm, 100 μm and 300 μm from layer boundary, respectively. As shown, all of the microstructures are composed of recrystallized or recovered UFGs with limited dislocation density, and there is no significant difference among them. Such homogenous microstructure can be attributed to the

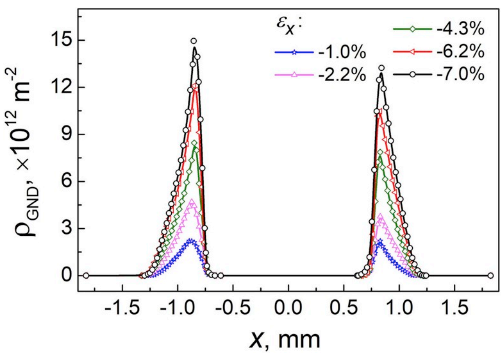

Fig. 8. The distribution of GNDs density, showing the accumulation in the near-interface zone with increasing strain.

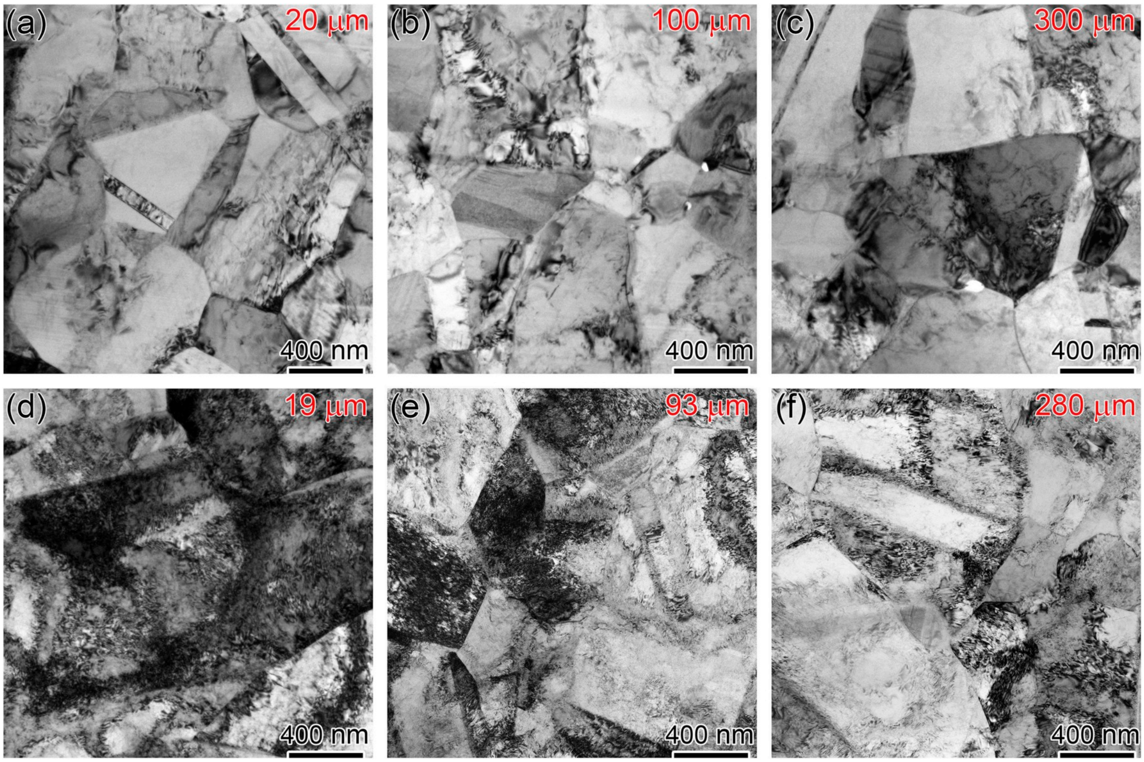

Fig. 9. Typical TEM micrographs observed in the UFG layer of laminates (a–c) before and (d–f) after tension, showing the deformation-induced gradient distribution of dislocation density in near-interface zone. The number at upper right corner of each subgraph represents the distance between observation region and layer boundary.

homogeneous thermal-plastic flow in the string zone during processing. Fig. 9(d–f) present the UFG microstructures at a tensile strain of ~14%. It is observed that the closest region (Fig. 9(d)) exhibits the most complex microstructure with extremely high dislocation density in both grain interior and near-grain boundary area, making the grain boundaries ambiguous. For the region with a distance of ~93 μm from layer boundary (Fig. 9(e)), dislocation density is obviously lowered, and the grain boundaries are relatively clear. With the increase of distance (Fig. 9(f)), dislocation density is further reduced, especially in the grain interior.

The multiple slip systems in polycrystalline materials makes it challenging to distinguish GNDs from statistically stored dislocations (SSDs), but the gradient variation of dislocation density demonstrates the intense storage of GNDs in near-interface zone (Ashby, 1970; Cheng et al., 2018). The complex microstructure shown in Fig. 9(d) suggests that the regions near to layer boundary experienced more serious plastic deformation under a higher stress level. The synergetic constraint induced by the incompatible deformation of CG and UFG layers changes the applied uniaxial stress to multiaxial stresses, which plays a role in promoting dislocation multiplication and entanglement (Asaro, 1983; Cheng et al., 2018; Wu et al., 2014a). Since the constraint stresses are higher as it gets closer to the layer boundary, it is logically reasonable that the regions closer to the boundary experience more serious deformation (Zhou et al., 2019). These results also emphasize that in the near-interface zone dislocation density gradient is caused by the synergistic deformation of incompatible layers. It should be noted that only a few of deformation twins were observed in UFGs, implying that dislocations dominated the plastic deformation of gradient interfaces.

4.4. Extraordinary strengthening effects of gradient interface

The hardness distributions of both laminate and freestanding samples measured at the tensile strain of ~14% are compared with that of as-prepared samples in Fig. 10(a). It is clear that two hardness peaks appear at the interfaces after tensile deformation. In Fig. 10(b), the blue data represents the hardness increment (ΔH) of laminate sample, and the red dotted line is a fitted ΔH distribution based on the ΔH of freestanding componential layers. It can be seen that big ΔH gaps (the green shadow regions) between the measured and fitted results appear in the near-interface zones, suggesting extra strain hardening retained in the strain gradient regions. This confirms that the enhanced flow stress and strain hardening rate found in laminate sample (Fig. 3) are largely caused by the strain gradient-related strengthening effects of gradient interface (Huang et al., 2018).

The GNDs accumulation in strain gradient zone affects dislocation activities in several ways. Firstly, GNDs act as local obstacles to mobile dislocations, i.e. playing a similar role as SSDs via. Taylor-type strengthening (σ_T) (Gao et al., 1999; Mughrabi, 2006)

$$\sigma_T = M\alpha\mu b\sqrt{\rho_s + \rho_G} \tag{7}$$

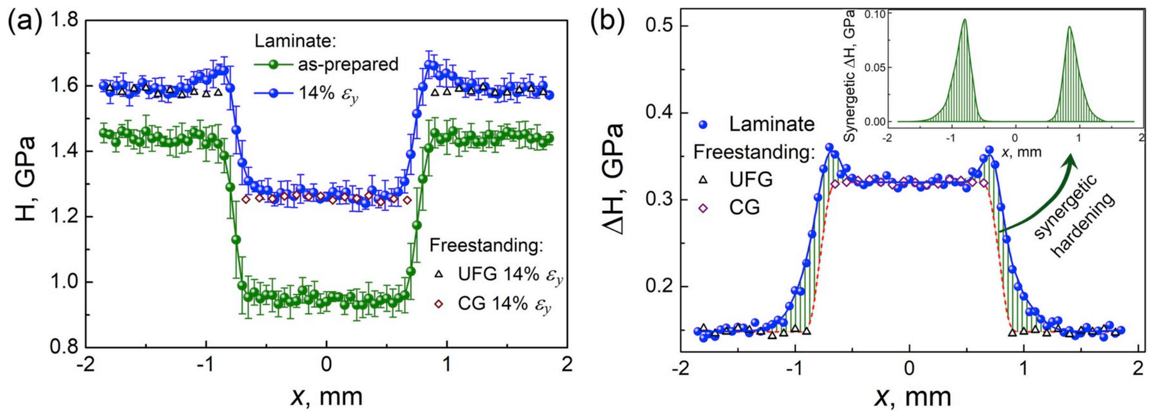

Fig. 10. (a) Hardness distribution of laminate, freestanding CG and UFG samples measured before and after tension. (b) The hardness increment (ΔH) of samples. The insert and the shadow region in (b) are the extraordinary hardness increment in the near-interface zone of laminate sample.

where M, α, μ and ρ_s are the Taylor factor, Taylor constant, shear modulus and density of SSDs, respectively.

Secondly, the gradient variation in spatial distribution of ρ_G is capable of producing a directional back stress (Ashby, 1970; Kassner et al., 2013; Voyiadjis and Song, 2019; Zhu and Lu, 2012), which reduces the resolved effective stress of dislocation slip in a long-range manner, thereby leading to back stress strengthening (Wu and Zhu, 2017). For the present laminate sample, the von-Mises equivalent back stress (σ_b) produced by local edge GNDs can be expressed as (Bayley et al., 2006; Li et al., 2017b)

$$\sigma_b = \sqrt{16\nu^2 - 16\nu + 7}\,\frac{\mu b R^2}{8(1-\nu)}\frac{\partial \rho_G}{\partial x} \tag{8}$$

where ν is the Poisson's ratio. R is the integral circular for GNDs to contribute to the back stress, which should be on the order of the characteristic material length associated with strain gradient plasticity (Gao et al., 1999; Huang et al., 2018).

Moreover, the long-range trapping effect of GNDs accumulation can help with accelerating the statistical storage of dislocations in the strain gradient zone during straining, which leads to a much higher density of SSDs. As verified in gradient nanotwinned Cu, the formation of GNDs distribution led to the rapid accumulation of SSDs, resulting in an exceptionally high total density of dislocations that was not reachable in a freestanding homogeneous counterpart, although GNDs density accounted for only a very small proportion of the total dislocation density (Cheng et al., 2018). This mechanism in heterostructure is encouraged by the synergetic constraint-induced multiaxial stresses which provides an opportunity to activate more slip systems (Asaro, 1983).

Considering the above strengthening mechanisms in a strain gradient zone, the extra flow stress ($\Delta\sigma$) generated from the gradient interface in CG/UFG laminate can be approximately calculated by superposing the contribution of each unite layer

$$\Delta\sigma = \sum_{i=1}^{n} f_i(\Delta\sigma_{Ti} + \sigma_{bi}) \tag{9}$$

and

$$\Delta\sigma_{Ti} = M\alpha\mu b(\sqrt{\rho_{si} + \rho_{Gi}} - \sqrt{\rho_{sialone}}) \tag{9.1}$$

$$\sigma_{bi} = \sqrt{16\nu^2 - 16\nu + 7}\,\frac{\mu b R^2}{8(1-\nu)}\frac{\Delta\rho_{Gi}}{\Delta x_i} \tag{9.2}$$

where f_i, ρ_{si}, ρ_{Gi} and $\Delta\rho_{Gi}/\Delta x_i$ represent the volume fraction, density of SSDs, density of GNDs and its average gradient of the ith layer, respectively. $\rho_{sialone}$ is the density of SSDs in a freestanding ith layer. These extraordinary strengthening effects around the gradient interface are responsible for the extra flow stress in Fig. 3(a). In addition, the gradual increase of GND pile-up also helps with maintaining high strain hardening rate (Fig. 3(b)), i.e. producing synergetic work hardening (Park et al., 2018; Wu et al., 2015).

4.5. Comparison of the extraordinary strengthening effects between gradient and sharp interfaces

Note that the strain gradient-dominated affected zone (~500 μm in width) of gradient interface is much wider than that (~10 μm) of the sharp NS/CG interface in roll-bonded laminate (Huang et al., 2018; Ma et al., 2016). Since both the superimposed back stress and extraordinary dislocation strengthening are higher as the strain gradient zone is wider (Eq. (9)), it is logically reasonable to expect that the wider the strain gradient zone around interface, the higher synergetic strengthening can be induced. These results may suggest that gradient interface is more efficient in producing synergetic strengthening.

The present UFG/CG laminate can be considered as a sandwich-structured composite with two discrete interfaces. Here data of the extra strength contributed by the gradient interface in CG/UFG/CG sandwiches (Wang et al., 2019), the sharp interfaces in UFG/CG/UFG and CG/NS/CG sandwiches (Liang et al., 2017; Ma et al., 2015) are collected and analyzed. Fig. 11 presents a comparison of

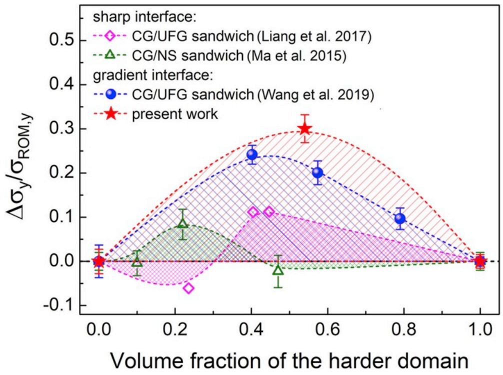

Fig. 11. Comparison of the synergetic strengthening effect between the gradient interface and the sharp interface in sandwich-structured laminates. The extra yield strength ($\Delta\sigma_y$) is normalized by dividing the prediction from rule of mixture ($\sigma_{ROM,y}$).

the synergetic strengthening effect between gradient and sharp interfaces. The normalized parameter $\Delta\sigma_y/\sigma_{ROM,y}$ is used to evaluate the synergetic strengthening in different materials, where $\Delta\sigma_y$ and $\sigma_{ROM,y}$ are the experimentally measured extra yield strength and the predicted yield strength using rule of mixture. It is clear that the sandwiches with gradient interface achieve much higher synergetic strengthening than the sandwiches with sharp interface.

If more gradient interfaces are introduced in the heterostructure, more pronounced synergetic effects could be obtained due to the increase of total volume fraction of strain gradient zone (Abu Al-Rub, 2008; Wu and Zhu, 2017). Since the synergetic interaction across interface is intrinsic to the deformation of heterogeneous domains with mechanical incompatibility, the macroscopic interface discussed here can also be viewed as an enlarged model interface for understanding the effects of microscopic interface in the structure composed of heterogeneous domains.

5. Conclusions

In summary, the effects of gradient interface on the strain behavior and mechanical responses of a CG/UFG laminate were studied by tensile test, height profile and DIC strain measurements, and microstructure observation. The main conclusions are summarized as below:

1) An enhanced strength-ductility synergy was found in the heterogeneous laminate, which can be primarily attributed to the extraordinary strengthening and work hardening effects originated from gradient interfaces.
2) The gradient interface plays a role in accommodating the strain incompatibility between layers via forming gradient strain distribution. The width of the zone with strain gradient remains a constant, whereas the intensity of strain gradient increases with increasing applied strain.
3) GNDs accumulation in strain gradient zone was theoretically derived and experimentally verified, which induces extraordinary strengthening by producing long-range back stress and promoting dislocation storage.
4) Owing to the formation of wider strain gradient zone around it, gradient interface is more effective than sharp interface in producing extraordinary strengthening.

Acknowledgements

This work was supported by the National Key R&D Program of China (2017YFA0204403), National Natural Science Foundation of China (No.11672195) and Sichuan Youth Science and Technology Foundation (2016JQ0047). Yanfei Wang would like to acknowledge the support from China Scholar Council.

References

Abu Al-Rub, R.K., 2008. Interfacial gradient plasticity governs scale-dependent yield strength and strain hardening rates in micro/nano structured metals. Int. J. Plast. 24, 1277–1306. https://doi.org/10.1016/j.ijplas.2007.09.005.
Asaro, R.J., 1983. Micromechanics of crystals and polycrystals. In: Adv. Appl. Mech. Elsevier 1–115. https://doi.org/10.1016/S0065-2156(08)70242-4.
Ashby, M.F., 1970. The deformation of plastically non-homogeneous materials. Philos. Mag. 21, 399–424. https://doi.org/10.1080/14786437008238426.
Bayley, C.J., Brekelmans, W.A.M., Geers, M.G.D., 2006. A comparison of dislocation induced back stress formulations in strain gradient crystal plasticity. Int. J. Solids Struct. 43, 7268–7286. https://doi.org/10.1016/j.ijsolstr.2006.05.011.
Chang, C.I., Lee, C.J., Huang, J.C., 2004. Relationship between grain size and Zener–Holloman parameter during friction stir processing in AZ31 Mg alloys. Scr. Mater. 51, 509–514. https://doi.org/10.1016/j.scriptamat.2004.05.043.
Chen, A., Li, D., Zhang, J., Song, H., Lu, J., 2008. Make nanostructured metal exceptionally tough by introducing non-localized fracture behaviors. Scr. Mater. 59, 579–582. https://doi.org/10.1016/j.scriptamat.2008.04.048.
Cheng, Z., Zhou, H.F., Lu, Q.H., Gao, H.J., Lu, L., 2018. Extra strengthening and work hardening in gradient nanotwinned metals. Science 362, eaau1925. https://doi.org/10.1126/science.aau1925.

Fang, T.H., Li, W.L., Tao, N.R., Lu, K., 2011. Revealing extraordinary intrinsic tensile plasticity in gradient nano-grained copper. Science 331, 1587–1590. https://doi.org/10.1126/science.1200177.

Gao, H., Huang, Y., Nix, W.D., Hutchinson, J.W., 1999. Mechanism-based strain gradient plasticity-I. Theory. J. Mech. Phys. Solid. 47, 1239–1263. https://doi.org/10.1016/S0022-5096(98)00103-3.

Huang, C.X., Wang, Y.F., Ma, X.L., Yin, S., Höppel, H.W., Göken, M., Wu, X.L., Gao, H.J., Zhu, Y.T., 2018. Interface affected zone for optimal strength and ductility in heterogeneous laminate. Mater. Today 21, 713–719. https://doi.org/10.1016/j.mattod.2018.03.006.

Huang, M., Fan, G.H., Geng, L., Cao, G.J., Du, Y., Wu, H., Zhang, T.T., Kang, H.J., Wang, T.M., Du, G.H., Xie, H.L., 2016. Revealing extraordinary tensile plasticity in layered Ti-Al metal composite. Sci. Rep. 6. https://doi.org/10.1038/srep38461.

Kassner, M.E., Geantil, P., Levine, L.E., 2013. Long range internal stresses in single-phase crystalline materials. Int. J. Plast. 45, 44–60. https://doi.org/10.1016/j.ijplas.2012.10.003.

Li, J.J., Lu, W.J., Zhang, S.Y., Raabe, D., 2017a. Large strain synergetic material deformation enabled by hybrid nanolayer architectures. Sci. Rep. 7. https://doi.org/10.1038/s41598-017-11001-w.

Li, J.J., Weng, G.J., Chen, S.H., Wu, X.L., 2017b. On strain hardening mechanism in gradient nanostructures. Int. J. Plast. 88, 89–107. https://doi.org/10.1016/j.ijplas.2016.10.003.

Li, J.S., Cao, Y., Gao, B., Li, Y.S., Zhu, Y.T., 2018. Superior strength and ductility of 316L stainless steel with heterogeneous lamella structure. J. Mater. Sci. 53, 10442–10456. https://doi.org/10.1007/s10853-018-2322-4.

Liang, F., Tan, H.F., Zhang, B., Zhang, G.P., 2017. Maximizing necking-delayed fracture of sandwich-structured Ni/Cu/Ni composites. Scr. Mater. 134, 28–32. https://doi.org/10.1016/j.scriptamat.2017.02.032.

Lu, X.C., Zhang, X., Shi, M.X., Roters, F., Kang, G.Z., Raabe, D., 2019. Dislocation mechanism based size-dependent crystal plasticity modeling and simulation of gradient nano-grained copper. Int. J. Plast. 113, 52–73. https://doi.org/10.1016/j.ijplas.2018.09.007.

Lyu, H., Hamid, M., Ruimi, A., Zbib, H.M., 2017. Stress/strain gradient plasticity model for size effects in heterogeneous nano-microstructures. Int. J. Plast. 97, 46–63. https://doi.org/10.1016/j.ijplas.2017.05.009.

Ma, X.L., Huang, C.X., Moering, J., Ruppert, M., Höppel, H.W., Göken, M., Narayan, J., Zhu, Y.T., 2016. Mechanical properties of copper/bronze laminates: role of interfaces. Acta Mater. 116, 43–52. https://doi.org/10.1016/j.actamat.2016.06.023.

Ma, X.L., Huang, C.X., Xu, W.Z., Zhou, H., Wu, X.L., Zhu, Y.T., 2015. Strain hardening and ductility in a coarse-grain/nanostructure laminate material. Scr. Mater. 103, 57–60. https://doi.org/10.1016/j.scriptamat.2015.03.006.

Mayeur, J.R., Beyerlein, I.J., Bronkhorst, C.A., Mourad, H.M., 2015. Incorporating interface affected zones into crystal plasticity. Int. J. Plast. 65, 206–225. https://doi.org/10.1016/j.ijplas.2014.08.013.

Ming, K.S., Bi, X.F., Wang, J., 2019. Strength and ductility of CrFeCoNiMo alloy with hierarchical microstructures. Int. J. Plast. 113, 255–268. https://doi.org/10.1016/j.ijplas.2018.10.005.

Mughrabi, H., 2006. Dual role of deformation-induced geometrically necessary dislocations with respect to lattice plane misorientations and/or long-range internal stresses☆. Acta Mater. 54, 3417–3427. https://doi.org/10.1016/j.actamat.2006.03.047.

Murr, L.E., 2016. Dislocation ledge sources: dispelling the myth of frank–read source importance. Metall. Mater. Trans. A 47, 5811–5826. https://doi.org/10.1007/s11661-015-3286-5.

Park, H.K., Ameyama, K., Yoo, J., Hwang, H., Kim, H.S., 2018. Additional hardening in harmonic structured materials by strain partitioning and back stress. Mater. Res. Lett. 6, 261–267. https://doi.org/10.1080/21663831.2018.1439115.

Voyiadjis, G.Z., Song, Y., 2019. Strain gradient continuum plasticity theories: theoretical, numerical and experimental investigations. Int. J. Plast (in press). https://doi.org/10.1016/j.ijplas.2019.03.002.

Wang, J., Zhang, R.F., Zhou, C.Z., Beyerlein, I.J., Misra, A., 2014. Interface dislocation patterns and dislocation nucleation in face-centered-cubic and body-centered-cubic bicrystal interfaces. Int. J. Plast. 53, 40–55. https://doi.org/10.1016/j.ijplas.2013.07.002.

Wang, Y.F., An, J., Yin, K., Wang, M.S., Li, Y.S., Huang, C.X., 2018a. Ultrafine-grained microstructure and improved mechanical behaviors of friction stir welded Cu and Cu–30Zn joints. Acta Metall. Sin. (Engl. Lett.) 31, 878–886. https://doi.org/10.1007/s40195-018-0719-3.

Wang, Y.F., Huang, C.X., Wang, M.S., Li, Y.S., Zhu, Y.T., 2018b. Quantifying the synergetic strengthening in gradient material. Scr. Mater. 150, 22–25. https://doi.org/10.1016/j.scriptamat.2018.02.039.

Wang, Y.F., Wang, M.S., Yin, K., Huang, A.H., Li, Y.S., Huang, C.X., 2019. Yielding and fracture behaviors of coarse-grain/ultrafine-grain heterogeneous-structured copper with transitional interface. T. Nonferr. Metal. Soc. 29, 588–594. https://doi.org/10.1016/S1003-6326(19)64967-8.

Wang, Y.F., Yang, M.X., Ma, X.L., Wang, M.S., Yin, K., Huang, A.H., Huang, C.X., 2018c. Improved back stress and synergetic strain hardening in coarse-grain/nanostructure laminates. Mater. Sci. Eng. A 727, 113–118. https://doi.org/10.1016/j.msea.2018.04.107.

Wei, Y.J., Li, Y.Q., Zhu, L.C., Liu, Y., Lei, X., Wang, G., Wu, Y.X., Mi, Z.L., Liu, J.B., Wang, H.T., Gao, H.J., 2014. Evading the strength–ductility trade-off dilemma in steel through gradient hierarchical nanotwins. Nat. Commun. 5, 1–8. https://doi.org/10.1038/ncomms4580.

Wu, H., Fan, G.H., Huang, M., Geng, L., Cui, X.P., Xie, H.L., 2017. Deformation behavior of brittle/ductile multilayered composites under interface constraint effect. Int. J. Plast. 89, 96–109. https://doi.org/10.1016/j.ijplas.2016.11.005.

Wu, S.W., Wang, G., Wang, Q., Jia, Y.D., Yi, J., Zhai, Q.J., Liu, J.B., Sun, B.A., Chu, H.J., Shen, J., Liaw, P.K., Liu, C.T., Zhang, T.Y., 2019. Enhancement of strength-ductility trade-off in a high-entropy alloy through a heterogeneous structure. Acta Mater. 165, 444–458. https://doi.org/10.1016/j.actamat.2018.12.012.

Wu, X.L., Jiang, P., Chen, L., Yuan, F.P., Zhu, Y.T., 2014a. Extraordinary strain hardening by gradient structure. Proc. Natl. Acad. Sci. U.S.A. 111, 7197–7201. https://doi.org/10.1073/pnas.1324069111.

Wu, X.L., Jiang, P., Chen, L., Zhang, J.F., Yuan, F.P., Zhu, Y.T., 2014b. Synergetic strengthening by gradient structure. Mater. Res. Lett. 2, 185–191. https://doi.org/10.1080/21663831.2014.935821.

Wu, X.L., Yang, M.X., Yuan, F.P., Wu, G.L., Wei, Y.J., Huang, X.X., Zhu, Y.T., 2015. Heterogeneous lamella structure unites ultrafine-grain strength with coarse-grain ductility. Proc. Natl. Acad. Sci. U.S.A. 112, 14501–14505. https://doi.org/10.1073/pnas.1517193112.

Wu, X.L., Zhu, Y.T., 2017. Heterogeneous materials: a new class of materials with unprecedented mechanical properties. Mater. Res. Lett. 5, 527–532. https://doi.org/10.1080/21663831.2017.1343208.

Yang, M.X., Li, R.G., Jiang, P., Yuan, F.P., Wang, Y.D., Zhu, Y.T., Wu, X.L., 2019. Residual stress provides significant strengthening and ductility in gradient structured materials. Mater. Res. Lett (in press).

Yang, M.X., Pan, Y., Yuan, F.P., Zhu, Y.T., Wu, X.L., 2016. Back stress strengthening and strain hardening in gradient structure. Mater. Res. Lett. 4, 145–151. https://doi.org/10.1080/21663831.2016.1153004.

Zeng, Z., Li, X.Y., Xu, D.S., Lu, L., Gao, H.J., Zhu, T., 2016. Gradient plasticity in gradient nano-grained metals. Extreme Mech. Lett. 8, 213–219. https://doi.org/10.1016/j.eml.2015.12.005.

Zhou, H., Huang, C.X., Sha, X.C., Xiao, L.R., Ma, X.L., Höppel, H.W., Göken, M., Wu, X.L., Ameyama, K., Han, X.D., Zhu, Y.T., 2019. In-situ observation of dislocation dynamics near heterostructured interfaces. Mater. Res. Lett. 7, 376–382. https://doi.org/10.1080/21663831.2019.1616330.

Zhu, L.L., Lu, J., 2012. Modelling the plastic deformation of nanostructured metals with bimodal grain size distribution. Int. J. Plast. 30–31, 166–184. https://doi.org/10.1016/j.ijplas.2011.10.003.

Zhu, L.L., Ruan, H.H., Chen, A.Y., Guo, X., Lu, J., 2017. Microstructures-based constitutive analysis for mechanical properties of gradient-nanostructured 304 stainless steels. Acta Mater. 128, 375–390. https://doi.org/10.1016/j.actamat.2017.02.035.